Chemical Engineering Journal 165 (2010) 946–957

Contents lists available at ScienceDirect

Chemical Engineering Journal

journal homepage: www.elsevier.com/locate/cej

Study of droplet size distribution during an emulsification process using *in situ* video probe coupled with an automatic image analysis

Abir Khalil [a,b], François Puel [a,b,*], Yves Chevalier [a,b], Jean-Marc Galvan [a,c], Alain Rivoire [a,b], Jean-Paul Klein [a,b]

[a] Université de Lyon F-69622, Lyon, France
[b] Université Lyon 1, Villeurbanne, CNRS, UMR5007, Laboratoire d'Automatique et de Génie des Procédés (LAGEP), CPE-Lyon, 43 bd du 11 Novembre 1918, 69100 Villeurbanne, France
[c] Université Lyon 1, Villeurbanne, CNRS UMR5270, Institut des Nanotechnologies de Lyon (INL), CPE-Lyon, 43 bd du 11 Novembre 1918, 69100 Villeurbanne, France

ARTICLE INFO

Article history:
Received 30 August 2010
Received in revised form 11 October 2010
Accepted 12 October 2010

Keywords:
Emulsification process
Drop size measurement
in situ monitoring
Image analysis
Multiphase mixing
Stirred vessel

ABSTRACT

Understanding the evolution of liquid–liquid dispersion is a key factor in operation and control of emulsification process. A dynamic tracking of an evolving droplet size distribution (DSD) in a dilute oil-in water (O/W) emulsion has been developed with the implementation of an *in situ* video probe dipped in a stirred vessel and coupled with an image analysis treatment. The optical probe allows real time recording of 2D images of the droplets. Recent image analysis software developed originally for an application in micromechanics was adapted and applied in delayed time on the video sequences regularly recorded. It automatically provided a measurement of the diameter of several thousands of droplets in the range of 10–100 μm. The relative accuracy on the droplet number average diameter was 10%. This measurement technique was then used to investigate at lab scale in a stirred vessel and in warm conditions the influence of several process parameters on the evolution with time of a dispersed melted cosmetic ingredient in a water solution containing a surfactant. The specific power input of stirring was the main parameter acting on the reduction of the mean droplet diameter and of the width of the DSD owing to its action on the droplet break-up mechanism. The surfactant concentration was a parameter of secondary relevance on the DSD probably due to the reduction of the coalescence rate and to a faster stabilization of the O/W interface. The use of a flat blade propeller instead of a Rushton turbine was preferable for the production of a narrower DSD. Finally the time required to reach equilibrium was found higher by a factor of 3–4 than predicted in the literature.

1. Introduction

Emulsions are common dispersed phase systems with diverse applications that include processed foods, polishes, waxes, agricultural sprays and road surfacing [1]. Since a decade, emerging applications require processes having an emulsification step. For instance, hydrophobic drugs are encapsulated in oil-in-water emulsions (O/W) and delivered to patients via oral administration, parenteral delivery, ophthalmic medicine and topical and transdermal creams [2,3]. Synthetic solid pigments are used in a wide range of personal care formulations in order to enhance their attractiveness (pearlescence, transparency, color, etc.). Their manufacturing process is based on the crystallization of an O/W emulsion with the presence of emulsifiers [4]. The control of the droplet size distribution (DSD) is a key issue since it ensures the reproducibility of the crystallization under confinement inside droplets. Consequently the control of evolving size distribution is an important feature of any production strategy [5,6].

Considerable research attention is focused on the study of such O/W emulsification process. Since several decades, some authors used the population balance equation (PBE) which provides a formal framework in which the evolution of the drop size distribution can be tracked. The prediction of DSD prepared in turbulently stirred reactors [5,7] or with high pressures homogenizers [8–13] is still in discussion. The key challenge associated with the implementation of predictive PBE models is the experimental determination of drop breakage and coalescence functions which represent the two main classes of mechanisms involved during emulsification. As highlighted by Sathyagal et al. [14] and O'Rourke and MacLoughlin [15] it requires reliable measurements of transient size distributions over extended periods in contacting configuration of practical interest.

A wide variety of experimental techniques have been utilized to monitor evolving DSD in agitated vessels. Techniques may be classified into two main classes. The first group is based on sam-

* Corresponding author at: Université Lyon 1, Villeurbanne, CNRS, UMR5007, Laboratoire d'Automatique et de Génie des Procédés (LAGEP), CPE-Lyon, 43 bd du 11 Novembre 1918, 69100 Villeurbanne, France. Tel.: +33 04 72 43 18 34; fax: +33 04 72 43 16 82.
E-mail address: puel@lagep.univ-lyon1.fr (F. Puel).

1385-8947/$ – see front matter © 2010 Elsevier B.V. All rights reserved.
doi:10.1016/j.cej.2010.10.031

pling procedure and an *ex situ* measurement is performed on the emulsion before it coalesces or when the emulsion is stabilized. The second group comprises *in line* observations (invasive or non invasive) which avoid sampling and dilution and allow measuring directly at the temperature and the pressure operating conditions. The advantages and limitations of the experimental techniques have been regularly evaluated in the literature. A complete review of the drop sizing methods used until the mid of this decade was given by O'Rourke and MacLoughlin [15] and Brown et al. [16]. From now on, *in situ* devices are commonly used. A comparison of three online measurement techniques based on laser techniques for drop size distributions in liquid/liquid dispersions was given by Maaβ et al. [6]. A large community of users applies the focused beam reflectance (FBRM) probe since it is well-suited for high of dispersed phase (up to 50% volume fraction). The main drawback of FBRM is that is does not actually measure the DSD but the Chord Length Distribution (CLD). One should therefore convert the measured CLD into its corresponding CSD which has been successfully demonstrated [17]. Recently a study has shown that FBRM tends to undersize droplets in emulsion [18]. Other laser back scattering techniques are still in test and evaluation. The principle of using back scattering techniques for measuring evolving drop size distributions is still asked, as very recently discussed by Maaβ et al. [6].

The use of a vision probe has remained the most reliable technique since it allows a direct visual observation. Recently it has been used to test the reliability of other techniques, such as laser back scattering techniques [18]. The earlier work devoted to the development of a video–microscope–computer technique for monitoring the drop size and size distribution was given by Pacek et al. [19,20]. A high-energy strobe light from a strobe flash was placed inside the vessel and in the vicinity of the wall within 2–8 mm. A stereo microscope linked to a video camera was placed outside in the vicinity of the vessel. The technique could provide valuable data, but was limited to the drops located close to the wall. Few years later, an endoscopic technique with a short focal distance was developed by [21] and could be dipped in the medium. In order to detect drops even in the stirrer region with velocities of about 1 m/s, a flash light with a period of 5 μs was used. At these velocities, the displacement was about 5 μm which is in the limit of resolution. The endoscope was connected to a CCD camera which took pictures of drops in the vicinity of the glass window at the bottom of the probe. Drop diameters from 30 μm up to 1000 μm could be detected at dispersed phase fraction up to 50% volume. A semi-automatic determination technique implying the validation of an operator was used to measure at least 200 drops per distribution in about 30 min. A similar system including a stereo-probe, a camera, a stroboscopic source and a PC equipped with frame grabber software was used by [22]. In the case of liquid–liquid dispersion of 1% cyclohexane mixed into water, the time evolution of the Sauter mean diameter for only two different stirring speeds has been presented. With the two latter probes, the visual observation is possible up to 50% volume fraction. If a quantitative determination of droplet size has to be performed by an automatic image analysis routine, the amount of dispersed phase is reduced to a few percents. Beyond it is rather difficult to separate droplets one another due to differences in the brightness through reflections, too many concentric droplets and overlapping contours of drops. Over a decade, our research group has developed *in situ* 2D imaging probes. They have been applied successfully in a stirred vessel to *in situ* monitor crystallization [23] in which a sampling is delicate since any cold point may trigger the birth of new crystals and also to measure size of droplets used as particle binder in a spherical agglomeration process [24]. From now on, specific improvements brought on the probes allow enhancing image quality so that it is possible to carry an automatic image analysis directly on the recorded frames. In the same time, in the field of micromechanics, a new algorithm of image analysis has been developed in order to estimate on line automatically the position of microspheres observed under microscopy [25]. Coupling a 2D imaging probe with such an automatic image analysis procedure allow acquiring in <1 min a large numbers of images of fast evolving liquid–liquid dispersions and measuring reliable droplet size distributions.

The aim of this study was first to test the use of coupling such hard and soft devices, and second to assess the influence of the process and physico-chemical parameters (type of stirrer, specific power input of stirring, surfactant-to-oil ratio) on the evolution with time of DSD during the emulsification process of a melted cosmetic ingredient in water in dilute conditions. The results obtained with this O/W emulsion will be confronted to previous ones presented in the literature.

2. Materials and methods

2.1. Model substance/raw materials

Ethylene glycol distearate (EGDS) of chemical formula is $C_{38}H_{74}O_4$ was purchased from Wako Chemicals. It is a cosmetic ingredient used in a wide range of personal care formulations in order to enhance their attractiveness (pearlescence, transparency, color, etc.). It was used as the model oil for this study. Its solubility in water was vanishingly small. Melting of EGDS took place in a narrow melting zone from 58 to 65 °C as analyzed by differential scanning calorimetry using a TA100® DSC instrument with heating at 2 °C min^{-1}. The density of melted EGDS was 858 kg m^{-3} at 78 °C. The interfacial tension between EGDS and water was measured at 70 °C by the pendent drop technique with a Krüss DSA10 tensiometer and was 5.62×10^{-3} J m^{-2}. The surfactant used for the oil stabilization was Brij 35P (tricosaethylene glycol dodecyl ether) from Fluka and had a melting zone from 38 to 41 °C. At room temperature its hydrophile lipophile balance HLB is 16.9. It allowed the formation of an O/W emulsion at the temperature of emulsification. Distilled water was used as the continuous phase. At 70 °C, its density and dynamic viscosity were respectively 977.4 kg m^{-3} and 3.9×10^{-4} Pa s.

2.2. Experimental set-up

The emulsification at constant temperature was carried out in a 1 L or 2 L double jacketed reactor (cylindrical vessel) as shown in [23]. In both cases, the reactor was equipped with condenser cooled with water to prevent evaporation of water. The temperature of the medium was measured using Pt-100 probe and was microcomputer controlled by manipulating the heating bath temperature set point. Four equally spaced stainless-steel baffles having a width of one tenth of the internal vessel diameter were used in conjunction with a speed-controlled mechanical stirrer in order to avoid vortex formation. The height of the emulsion H was equal to T. The stirrer was located at a distance of $H/3$ above the vessel base.

Two types of mechanical stirrer were tested: an axial flow profiled three flat blades propeller Mixel TT® and a standard six blades Rushton turbine. Tables 1 and 2 present a sketch and the dimensions of the stirrers relatively to the internal vessel diameter T. Their respective values and expressions of power number and mean circulation time are given in Section 3. Each stirrer was employed in its practical application range expressed by it specific power input ε: from 200 to 500 W/kg in the case of the flat blade propeller and from 500 to 1000 W/kg for the Rushton turbine. The power input of the flat blade propeller was limited by entrainment of air bubbles that were clearly visualized by the video probe beyond 500 W/kg.

Table 1
Mixell TT® flat blade propeller design.

Dimension	Ratio of dimensions
Internal vessel diameter T	T
Total stirrer diameter D	3/5T
Blade thickness	D/50
Number of profiled blades	3
Angle between 2 blades	120°

(T = 0.11 m for a 1.0 L vessel; T = 0.15 for a 2.0 L vessel).

An upper liquid oil layer remained at the surface of the medium when the power input of the turbine was below the lower limit. The operator visually checked that the distribution was uniform for all the stirring rates.

An *in situ* video microscope probe EZ Probe-D25® designed in our laboratory was immersed in the reactor (see Fig. 1). It was located at 5 cm above the stirrer, close to the stirring shaft, with a vertical angle of about 30°. At this point, the flow moved downwards before being aspired by the stirrer. This position is one of the probe locations recommended in the literature [16]. This probe is an evolution of a previous one used to monitor crystallization and agglomeration processes [23,24]. The first improvement was brought by the use of a Light Emitting Diode (LED) back lighting driven by a pulse generator triggered by the video camera. This brought a flash light synchronized with the recording of the video camera to a gap of several hundreds of micrometer width where the emulsion flowed. The blurring by motion was eliminated by a pulse illumination of 50 μs. The back-lighting allowed the visualization of droplet shadows which appear in black on a white background. The choice of a diascopic observation allows generating a consistent background which facilitates the automatic image analysis carried on the frames. The transmitted light illuminated a CCD video camera. The use of a remote head monochrome CCD camera having a recording rate of 50 frames per second was the second decisive improvement. The frame has the following specifications: image of size 640 × 480 pixels, resolution up to 2.0 μm, 256 grey levels. This resulted in an optical field of 1300 μm × 960 μm. It allowed the detection of droplets having a diameter above 8 μm. Each frame contained several tens of droplets as shown in Fig. 2. An USB video grabber retrieved the video data, compressed it if necessary and sent it to a computer. This probe allows real time acquisition of 2D images of the droplets generated during the emulsification process.

2.3. Batch operating conditions

EGDS, water and surfactant were poured at room temperature in the reactor. The weight fraction of oil phase was 0.2%. The vessel was then heated up to 70 °C and kept at this temperature. At the low stirring speed of 150 rpm, the full content of melted EGDS remained above the aqueous phase; no droplet was detected by the video probe located in the vicinity of the stirrer. Emulsification started with an elevated stirring rate during 5 s (power input of 2 W/kg) allowing the dispersion of the oil layer in the water phase for this short time. Then the stirring speed was adjusted to a value corresponding to the desired specific power input.

The influence of the specific power input ε and of the surfactant-to-oil ratio was investigated for each stirrer. Three values (low, intermediate and high) of ε covered the application range of the stirrer (see precisely Section 2.2). Considering that a molecule of surfactant may cover 50×10^{-20} m^2 of the interfacial area, 6 mg of surfactant was an estimate of the minimum amount required for full coverage of the interface of a population of monodisperse droplets of 20 μm (lowest size detected) in a total volume of 2 L. The amounts of surfactant introduced in the medium (from 0.4 g to 4 g) were far beyond this minimum value and below the critical micelle concentration. They were corresponding to three different surfactant-to-oil weight ratios from 0.1 to 1. The whole experimental protocol results in 18 operating conditions summarized in Table 3.

2.4. Automatic image analysis

A video sequence of 30 s was regularly recorded during the run. A posteriori image analysis treatment was automatically performed. It is based on an algorithm developed by Peng et al. [25]

Table 2
Rushton turbine design.

Dimension	Ratio of dimensions
Internal vessel diameter, T	T
Total stirrer diameter, D	T/2
Disc diameter	3/4D
Disc thickness	D/50
Blade thickness	D/50
Blade height	D/5
Total blade depth	D/4
External disc blade depth	D/8
Internal disc blade depth	D/8
Number of blades	6
Angle between 2 blades	60°

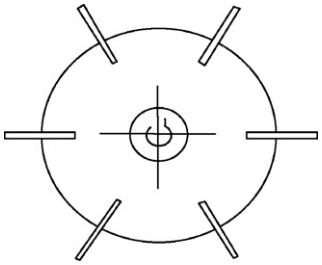

(T = 0.11 m for a 1.0 L vessel; T = 0.15 for a 2.0 L vessel).

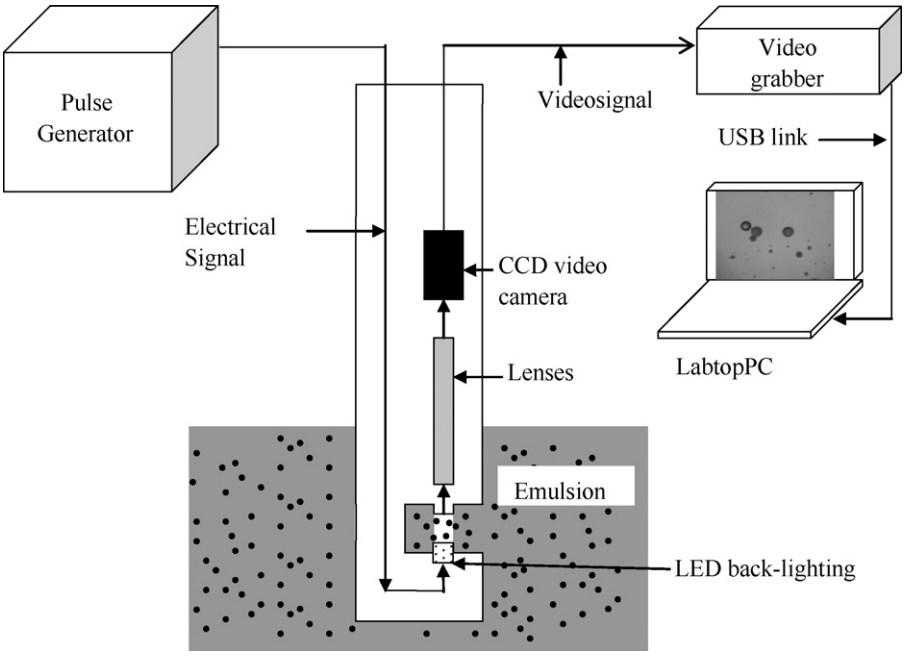

Fig. 1. Sketch of the video probe immersed in the emulsion.

for the monitoring of microspheres which were components in an assembly workspace in micromechanics. The procedure required to process the data consisted of three main parts: (1) extract one image over five ones in order to avoid taking into consideration a droplet several times. 300 frames were selected for each recording; (2) detect the circular patterns of the droplets with the use of a circular Hough transform as proposed by Illingworth and Kittler [26,27] and transform them to circles. Three sub-steps were necessary: (2i) compute the gradient field of the image in the specified regions; (2ii) transform the gradient field to an accumulation array; (2iii) locate the positions of the centers of the circles in the accumulation array; (3) estimate the radius of the circles by two sub-steps; (3i) compute the signature curve for each circle identified in image; (3ii) estimate the radius by matching its signature curve to the "standard" signature curve of a circle.

The droplet size range decreased with time during an emulsification until it reached equilibrium. In order to have a consistent precision, the size measurement range was limited to 10–90 μm. The accuracy was poor below 10 μm since the resolution was 2.0 μm per pixel. Beyond 90 μm, the frequency of wrong detection due to the simultaneous detection of several gathered droplets was significant. In practice, a set of five parameters must be tuned in the software used for the image analysis treatment. This was done by comparing qualitatively the raw and the processed frames on different video sequences taken from three different runs. Three sets of parameters were obtained. For each parameter, the fitted values differed relatively in a range of 15% around a mean one. A mean set of parameters obtained by averaging the values was kept for the automatic analysis of the frames collected in all the experiments. Fig. 2 displays a raw image, the numerical values of each pixel in the accumulation array and the image after treatment. The largest values in the accumulation array (see Fig. 3b) correspond to the positions of the circle centers. Red crosses and green circles display respectively the centers and the perimeters of the selected droplets (see Fig. 2c) (For interpretation of the references to color in this text, the reader is referred to the web version of the article.). Droplets connected with the edges of the image, concentric droplets, small dots in the raw image (too small droplets and blurred droplets located outside of the depth of field) were missing in the population of the selected droplets (see Fig. 2c).

5000 until 20,000 droplets were taken into consideration for each video sequence recorded which is far beyond the minimal requirement of about 500–1000 droplets proposed in the literature [15,16,19]. It was then possible to plot the time evolution of the number probability density function of the droplet population, and to calculate the number averaged diameter ($d_{1,0}$) and the variation coefficient (VC_N defined as the ratio of the standard deviation to the number averaged diameter) of the DSD. In the case of regular sphere-like droplets, the volume distribution could be easily computed and their features (volume average diameter $d_{4,3}$ and variation coefficient VC_V) extracted. The Sauter mean diameter $d_{3,2}$

Table 3
Operating conditions of the emulsification experiments.

Run number	Stirrer	Specific power input (W/kg)	Surfactant-to-oil ratio (weight)	Run number	Stirrer	Specific power input (W/kg)	Surfactant-to-oil ratio (weight)
AK26	Flat blade Propeller	0.2	0.1	AK30	Rushton Turbine	0.5	0.1
AK27		0.35		AK32		0.75	
AK28		0.5		AK31		1.0	
AK19		0.2	0.5	AK35		0.5	0.5
AK24		0.35		AK36		0.75	
AK20		0.5		AK37		1.0	
AK17		0.2	1.0	AK38		0.5	1.0
AK22/AK23		0.35		AK39		0.75	
AK18		0.5		AK40		1.0	

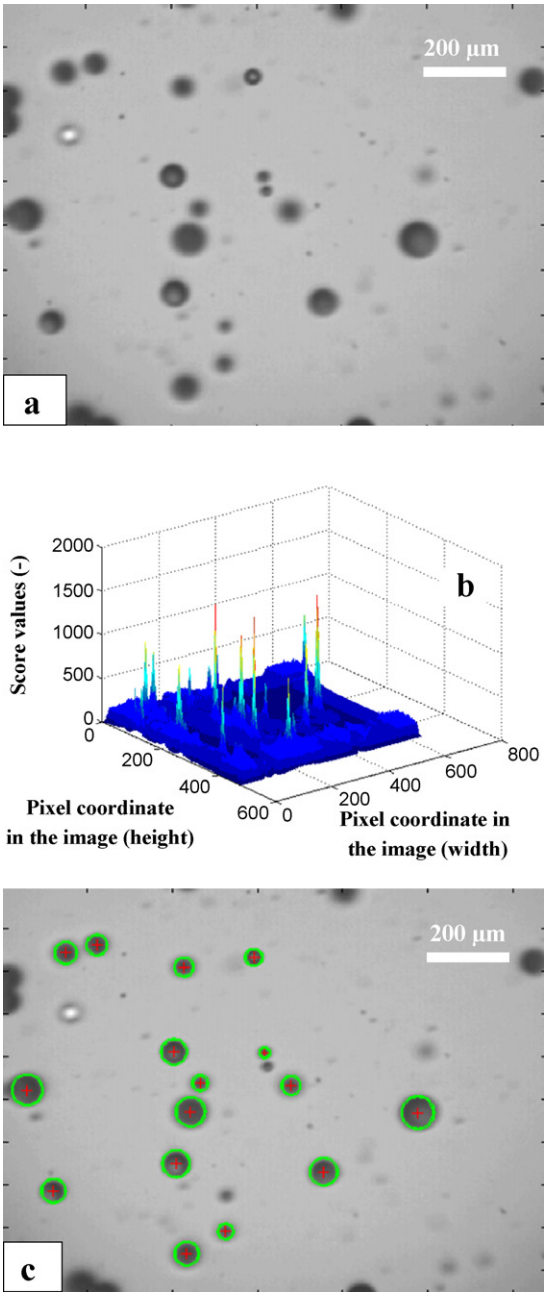

Fig. 2. Selection of droplets by the automatic image analysis treatment: (a) raw image, (b) score values of the accumulation array and (c) treated image with selected droplets.

was also obtained since it is directly related to the specific area of the dispersed phase and commonly used in studies for displaying the DSD.

The treatment of a 300 frames required about 40 min. It is clear that such processing time was too large to allow real time image analysis and DSD calculation during an experiment. The DSD measurement was performed in delayed time. According to the operating conditions chosen, a video sequence of only 30 s was sufficient to obtain enough representative data of the DSD. Depending on the dynamics of the emulsification process, it was possible to track every minute the evolution of the liquid–liquid dispersion. Since the video probe could be immersed in a stirred vessel, it was possible to follow very easy emulsification process at lab scale in industrial conditions of temperature profile and stirring.

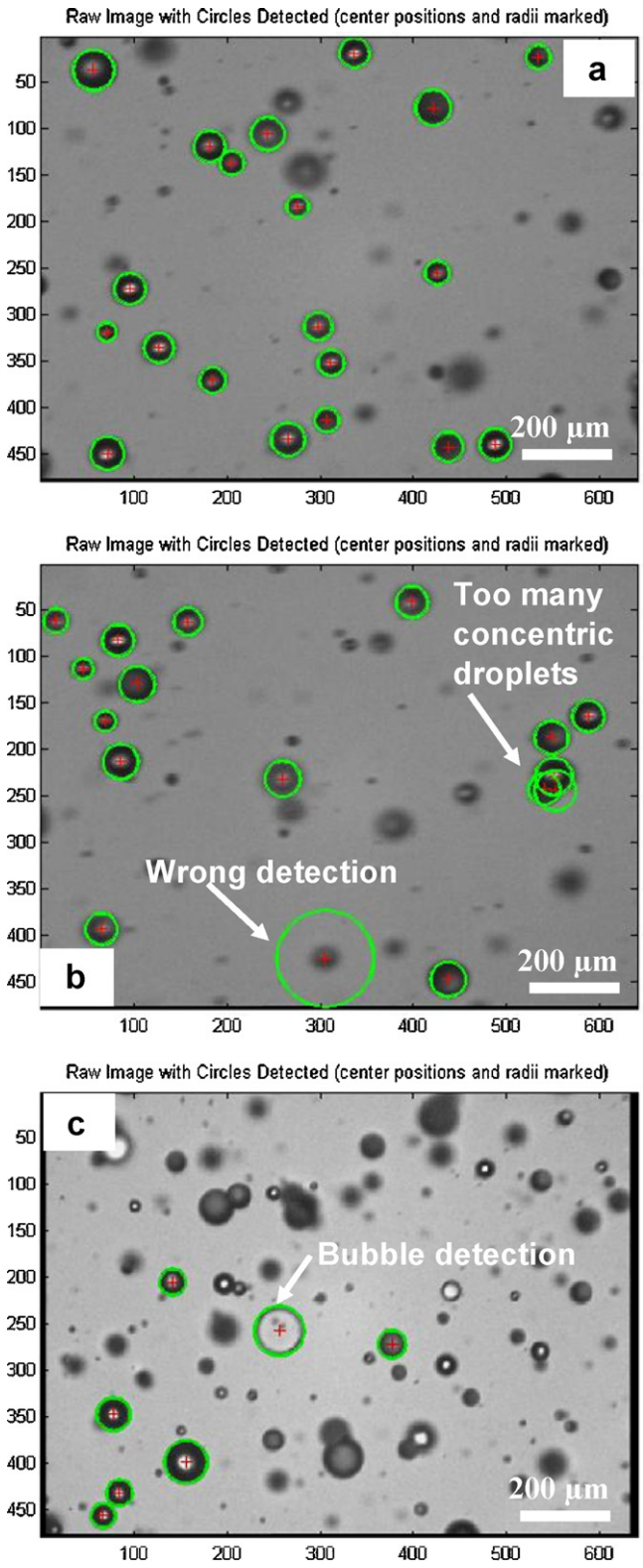

Fig. 3. Different cases of droplet detection before the count (a) any error, (b) errors coming from a wrong detection and with several concentric droplets and (c) detection of a bubble present in the medium.

3. Theoretical considerations about the influence of stirring on liquid–liquid dispersion

Flow regimes are classified according to the value of the dimensionless Reynolds number Re which represents the ratio of inertial to viscous forces:

$$Re = \frac{\rho_C \ N \ D^2}{\mu_C} \tag{1}$$

where ρ_C (kg m^{-3}) and μ_C (Pa s) relatively density and dynamic viscosity of the continuous liquid phase, D diameter of the stirrer (m), N the stirrer rotational velocity (s^{-1}). Laminar conditions exist when $0 < Re < 10$, transition flow occurs when $10 < Re < 10^4$ and fully turbulent flow regime when $Re > 10^4$.

The specific power input ε (W/kg) represents the average energy dissipation rate brought by the stirring system. It was calculated by dividing the power consumption P (W) by the total mass of the emulsion:

$$\varepsilon = \frac{P}{\rho_C V_T} \tag{2}$$

$$P = N_P \rho_C N^3 D^5 \tag{3}$$

where N_p the dimensionless power number of the stirrer. The power number values used for the Rushton turbine and the flat blade propeller were respectively 5.0 [28] and 0.8 [29].

The tank mean circulation time t_{circ} is the time a flow element spends to steadily pass through the stirrer. It depends on the stirrer, the vessel geometry and the type of flow regime. In the case a stirred vessel in turbulent flow conditions, the mean circulating time is calculated using the following correlations [30]:

$$N \cdot t_{circ} = 6\left(\frac{T}{D}\right)^2 \quad \text{for an axial flow stirrer} \tag{4}$$

$$N \cdot t_{circ} = 4\left(\frac{T}{D}\right)^2 \quad \text{for a Rushton turbine} \tag{5}$$

where T the internal diameter of the vessel (m)

A turbulent flow regime was obtained for all the hydrodynamic conditions chosen in this study (see Table 4). Turbulence involves innumerable, various sized eddies or swirling flow motions. According to Kolmogorov theory of local isotropic turbulence [31], the energy spectrum of eddies depends on the rate of energy dissipation ε and the kinematic viscosity ν_C of the continuous liquid phase. Large eddies decay to small eddies. The scale of large eddies denoted macroscale l_{macro} can be approximated by the width of the fluid ejected by the agitator, i.e. the width of the stirrer blade [32]. On the other hand, the scale of small eddies denoted microscale l_{micro} is independent of agitator and tank size and is defined as:

$$l_{micro} = \left(\frac{\nu_C^3}{\varepsilon}\right)^{1/4} \tag{6}$$

where ν_C is the kinematic viscosity of the continuous liquid phase (m^2 s^{-1}).

The Weber number We is a dimensionless number that is widely used in the case of emulsification. It takes into account the balance between break-up and coalescence of the droplets. It represents the ratio of the driving force causing partial disruption to the resistance due to interfacial tension. Increased Weber number is associated with a greater tendency for droplet deformation to occur at higher shear. Depending on the flow regime of the continuous liquid phase around the droplet, many expressions of the Weber number arise. In a stirred vessel, in a turbulent flow regime when the inertial forces are higher than the viscous effects ($Re > 10^4$) the Weber number is expressed as:

$$We = \frac{\rho_C \cdot N^2 \cdot D^3}{\sigma} \tag{7}$$

where σ (Jm^{-2}) is the interfacial energy at the droplet interface.

The early studies of Hinze [33] and Shinnar [34] have related the maximum stable droplet size d_{max} to the maximum local energy dissipation rate ε_{max} in a stirred vessel, in the case of a dilute turbulent dispersion in which the break-up phenomena is the dominating phenomenon. For a droplet diameter higher than d_{max}, the droplet does not resist further break-up. Lasigetty et al. [35] has given a relationship allowing the prediction of d_{max} in the case of two inviscid fluids mechanically stirred by a Rushton turbine in a vessel:

$$\frac{d_{max}}{D} = 0.125\, We^{-0.6} \tag{8}$$

Leng and Calabrese [36] have reported on their review that the mean energy dissipation rate ε was assumed to be proportional to its maximum value ε_{max} and at equilibrium $d_{max} \propto d_{3,2}$. With these assumptions and by combining the expressions (1), (2) and (7), it is easy to demonstrate that

$$d_{3,2} \propto \varepsilon^{-0.4} \tag{9}$$

Table 4 summarizes the values of the Reynolds and Weber numbers, the mean circulating time, the microscale and the maximum stable droplet size for all the operating conditions.

4. Results and discussion

The first part is devoted to assess the reliability of the *in situ* sizing technique. Then the influence of several process parameters on the emulsification process is presented and discussed. Additional comparisons with the literature ended this section.

4.1. Assessment of the in situ sizing measurement technique

4.1.1. Total volume of droplets taken into account by the size measurement technique

Video sequences were recorded regularly in an experiment. The same number of frames were analyzed for each sequence. As far as the emulsification was in progress, the number of droplets increased and their diameters decreased. According to the mass balance, the total volume of droplets must remain constant in this batch mode. For each video sequence during a run, the total volume of droplets from the number DSD was calculated. Its relative variation from one measurement to the other was at the most 5%. It could reasonably be considered that the mass balance was respected. For runs carried on at low specific power inputs (0.2 and 0.5 W/kg respectively for the flat blade propeller and the Rushton turbine) the calculated total volume of droplets could be varied by more than 20% in the earlier moments of emulsification (for instance at 10 min). This may be explained by the fact that few large droplets of diameter above 90 μm that were still present at the beginning and had not been counted although their relative contribution to the total volume was very important. In a number distribution, the impact of such droplets was much lower. Such few DSDs of the beginning were not discarded. The total volume of droplets was almost constant from one run to the other. The mean value was 3.8×10^8 μm^3 and its variation was <5%. This gives evidence that, despite different circulating flow rates were applied, the measurement procedure was independent of the flow motion features in the analysis zone. The volume fraction of dispersed liquid phase necessary for the determination of the DSD was 0.016% and 0.008% respectively for the 1 Land 2 L vessel. This small fraction representing several thousands of droplets was considered

Table 4
Calculated values of the Reynolds Number Re, the mean circulating time t_{circ}, the Weber Number We, the maximum droplet size d_{max} and the minimum size of eddies l_{micro} in the different hydrodynamic experimental conditions (see mathematical expressions in Section 3).

Stirrer and volume of the vessel	Specific power input ε (W/kg)	Stirring rate N (rpm)	Reynolds Number Re (–)	Mean circulating time t_{circ} (s)	Weber number (–)	Maximum droplet diameter d_{max} (μm)	Microscale l_{micro} (μm)
Flat blade propeller 2 L	0.2	265	8.9×10^4	3.6	1347	–	24
	0.35	320	1.1×10^5	3.0	1964	–	21
	0.5	360	1.2×10^5	2.7	2486	–	19
Rushton turbine 1 L	0.5	340	3.8×10^4	3.1	808	118	19
	0.75	390	4.3×10^4	2.7	1063	100	17
	1.0	430	4.7×10^4	2.5	1293	89	16

as enough to correctly represent the entire dispersed phase. This *in situ* size measurement may be considered as consistent since the mass balance and the volumetric concentration of dispersed liquid phase were found constant whatever the operating conditions of stirring.

4.1.2. Assessment of measurement error rating of droplets and impact on the mean number diameter

With the use of a mean set of image analysis parameters, a small part of droplets visualized in the frames were misinterpreted. This occurred either when more than two concentric droplets were superimposed in the images, or when air bubbles were counted as oil droplets (see a few examples in Fig. 3). On the runs AK24 and AK36 carried out respectively with a flat blade propeller and with a Rushton turbine, the image analysis was verified visually by the operator on every frame selected for all the video sequences recorded. An error rating was defined as the relative number of wrong droplets that have been selected and measured. This number error rating varied from 2.6% to 5.6% for a video sequence. The mean error rating was about 3.9% whatever the stirrer used. The modification of the stirrer did not bring any significant difference on this error rating, since the flow motion in the analysis zone visualized thanks to the motion of the droplets was similar. At least, the impact of this error rating on the droplet mean number diameter was assessed to be about 5%.

4.1.3. Assessment of the accuracy of the diameter measurement

Another uncertainty may come from the evaluation of the diameter of the droplets. Different tests performed showed that the error was at the most two pixels. According to the resolution of 2.0 μm per pixel, a maximal absolute error was 4.0 μm. Considering a whole size distribution, a relative maximum error on the number-averaged diameter could be calculated. For the size measurements carried on during the run AK24, such error varied from 7.1% to 12.5% with a mean value of 10.3%. This relative accuracy of the diameter measurement with this *in situ* measurement technique was considered as satisfactory since other ones (like laser scattering techniques) for measuring evolving drop size distributions in liquid/liquid system are still in debate.

4.1.4. Assessment of the accuracy of the DSD measurement with calibrated spheres

A suspension of calibrated microspheres of polystyrene used for the calibration of a laser diffraction size measurement technique was selected. It had a mean diameter of 39.6 μm with a standard deviation of 1.5 μm since it corresponded to a common value of mean droplet size obtained in this study. This suspension was dispersed in water under stirring in the reactor at ambient temperature. It was not possible to observe the suspension at the emulsification temperature, since microspheres aggregated in warm conditions. A video sequence was recorded at room temperature and the images were automatically analyzed with the parameters fitted for the droplet size measurement. Fig. 4 displays a recorded frame and the histogram of the measured microsphere diameter distribution. The calculated average size and standard deviation were 39.5 μm and 2.6 μm respectively. These results are close to the diameter distribution features of the calibrated microspheres. The same optimized set of image treatment parameters were kept for the whole study.

4.1.5. Assessment of the reproducibility of an emulsification run

The assessment of the reproducibility of the emulsification procedure and of the DSD measurement was done by comparing the DSD obtained in two runs carried out in the same conditions (see Fig. 5). At the earlier times of emulsification (10 min), the mean relative discrepancy between two DSD measurements was about 7%. It decreased down to 3% until a stable distribution was reached. The emulsification procedure and the droplet size measurement were then considered as satisfactorily reproducible.

4.2. Study of the emulsification process

4.2.1. Evolution of the DSD during an emulsification batch run

The evolutions with time of the DSD measurements for two representative batch runs (AK24 and AK36) respectively carried out

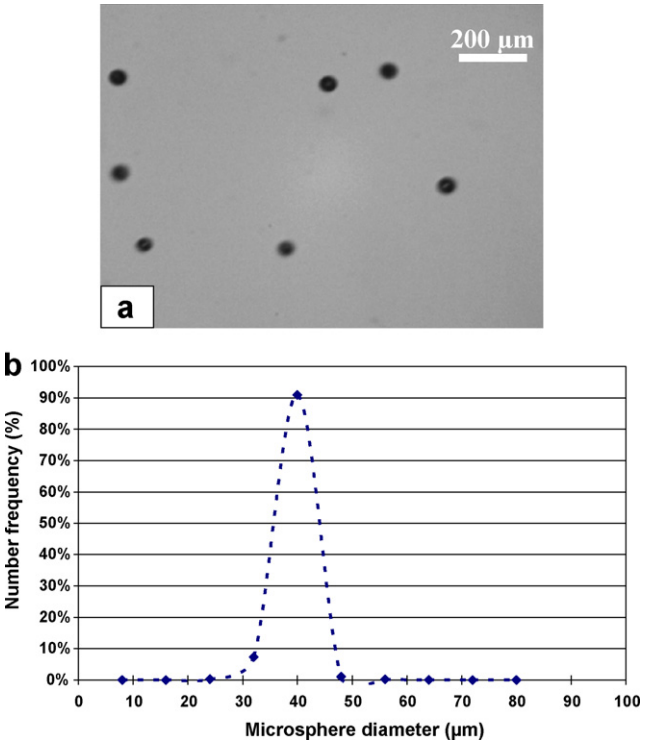

Fig. 4. Measurement of microsphere diameter (a) frame of microspheres under observation (size of the picture 1300 μm by 960 μm) and (b) number frequency histogram of the microsphere diameter.

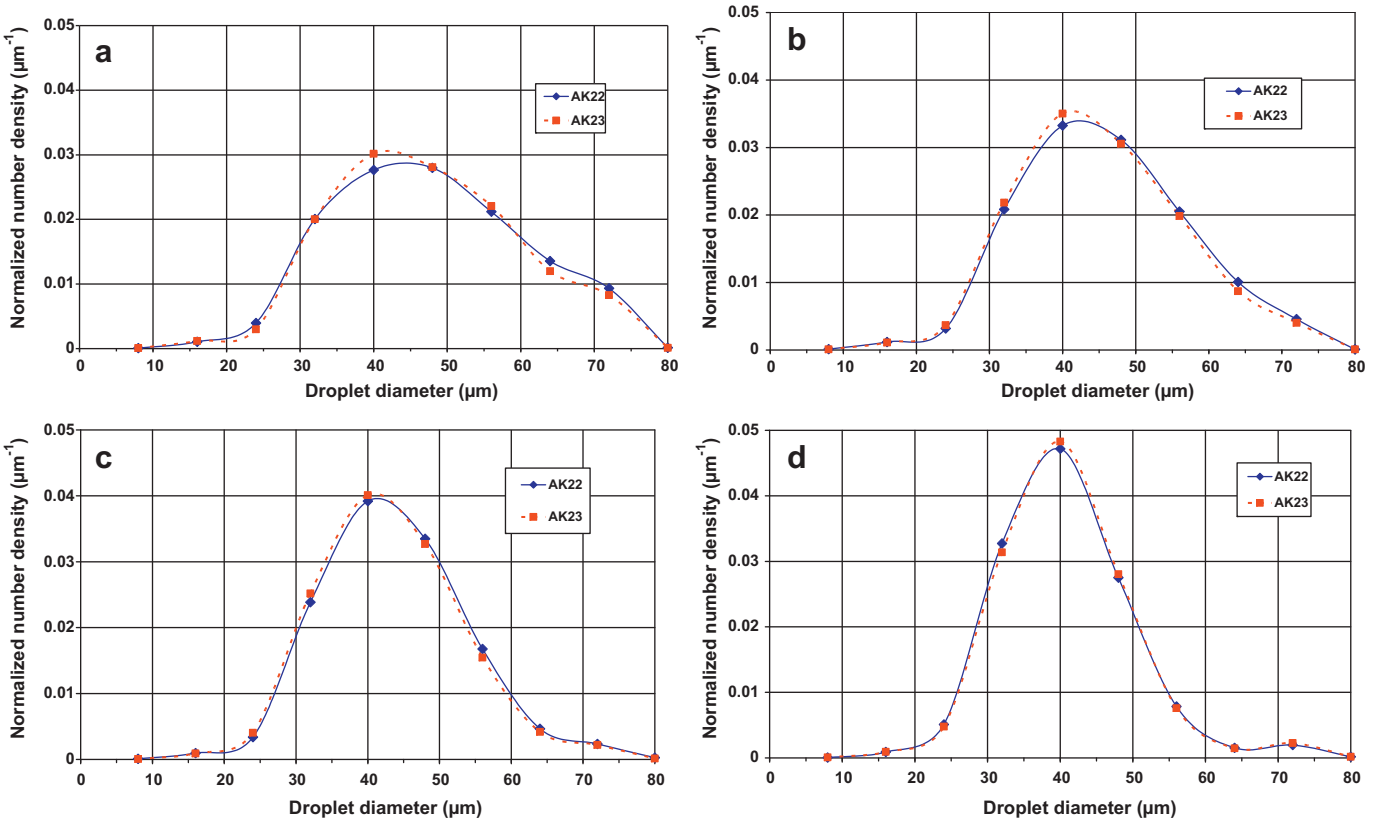

Fig. 5. Reproducibility of DSD measurement: comparison of the population number density distribution at different times for the runs AK22 and AK23 stirred with a flat blade propeller and carried out with the same operating conditions (a) 20 min; (b) 40 min; (c) 80 min; (d) 180 min.

with the flat blade propeller and the Rushton turbine are plotted in Fig. 6. For all the runs, the DSD remained mono-modal (one population) since the stirring rates were chosen in the industrial application range of these two stirrers. An increase of the stirring rates may cause a second peak to appear in the distribution [37] and brought about gas bubbles in the medium, leading to false detection of droplets by the image analysis treatment. The smallest droplet sizes were quickly detected during the emulsification and were in the range of 10–25 μm. Their values remained constant. In the same time, the fraction of smallest droplets steadily increased. On the contrary the larger droplets broke up due to the flow motion generated by the stirrer and their fraction regularly decreased. The rate of reduction of the mean diameter and of the distribution width was significant during the first 2 h of the emulsification since the fraction of large droplets which could be broken was large. During the following hours, the DSD was slowly shifted to smaller sizes and the distribution width progressively became narrower. It could be explained by a progressive reduction of the break-up rate as far as the fraction of large droplets was reduced. Depending on the operating conditions, reaching a stable distribution might require at least 3 h.

4.2.2. Influence of the investigated parameters on the DSD

The influence of the three investigated parameters on the DSD was assessed by plotting the evolution with time of the calculated number-average diameter and of the variation coefficient over all the runs (Fig. 7). The features of the number and volume size distributions when the equilibrium was reached are also presented in Table 5.

The increase of the specific power input allowed reducing significantly the number mean diameter and the coefficient variation of the DSD. The impact of specific power input has been already

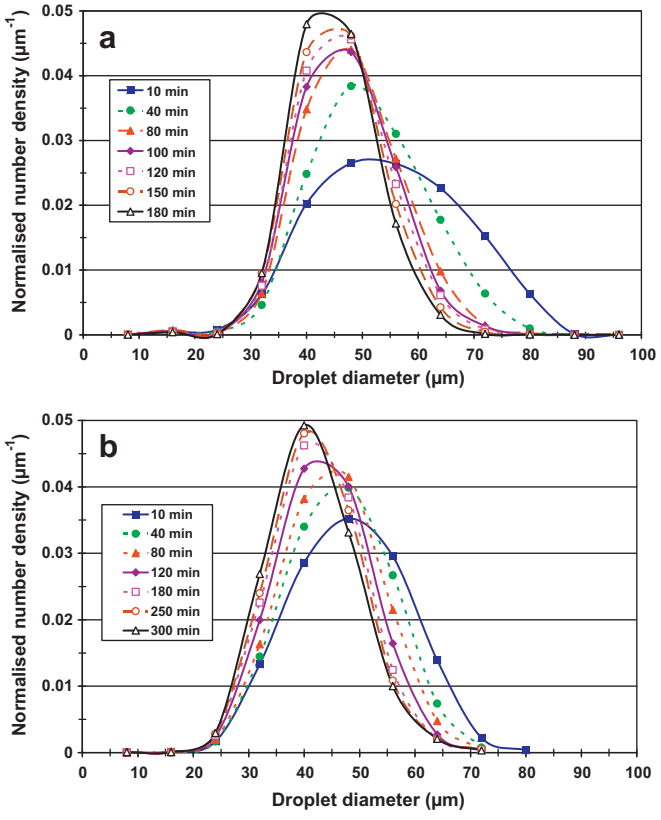

Fig. 6. Evolution with time of the normalized number density: (a) run AK24 stirred with a flat blade propeller and (b) run AK36 stirred with a Rushton turbine.

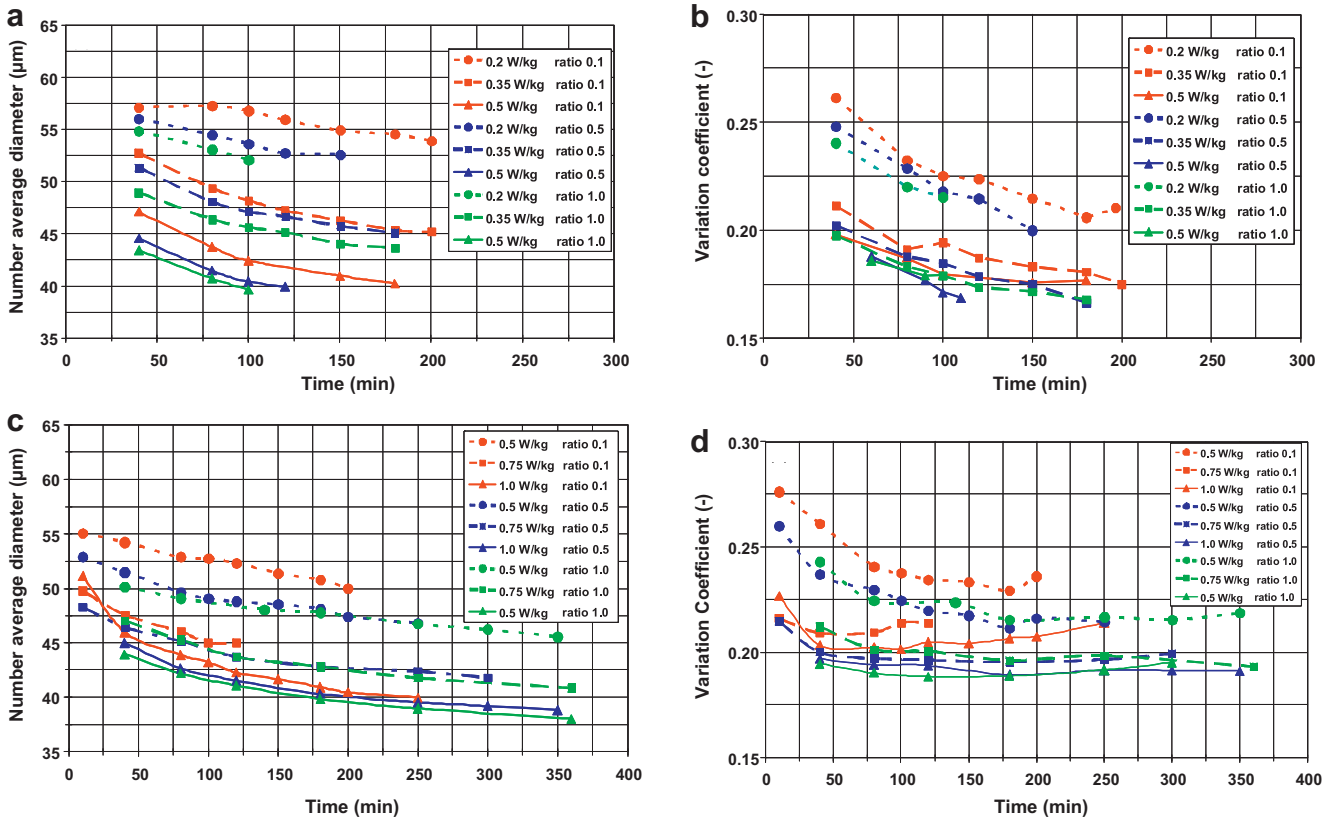

Fig. 7. Evolution with time of the number DSD features (number average diameter and variation coefficient) for runs carried on with a flat blade propeller (a) and (b) and with the Rushton turbine (c and d); specific power input respectively for flat blade propeller and Rushton turbine (●: 0.2 and 0.5 W/kg; ■: 0.35 or 0.75 W/kg; ▲: 0.5 or 1.0 W/kg); surfactant-to-oil weight ratio (dotted line: 0.1; dashed line: 0.5; solid line: 1.0).

pointed out by the earlier works of Chatzi et al. [38] and was reported by several authors in the literature [36,38]. The impact of the specific power input is quite easy to explain since higher turbulence intensity is more effective in breaking the drops [16,36]. The increase of the surfactant-to-oil ratio had a favorable impact on the reduction of the mean droplet diameter. It also caused the size distribution to sharpen, but to a lesser extent. Possible explanations on the role of the surfactant content lie in the fact that the coalescence rate was reduced when the droplets were in quiescent regions far from the stirrer dispersion zones and the presence of a larger surfactant amount allowed a faster stabilization of the O/W interface [36,40]. From these observations, we could underline that in this study the first order parameter acting on the DSD features appeared to be the specific power input, the surfactant-to-oil ratio acting as a parameter of a secondary importance.

The type of the stirrer had only a slight influence on the DSD evolution with time. The use of Rushton turbine allowed a quicker reduction of the mean size and of the distribution width during the first hour of emulsification. This could be explained by the fact that the Rushton turbine operates a higher specific power number than the flat blade propeller, and provides higher shear and turbulence level with lower pumping, leading to a faster droplet break-up. After few hours of emulsification, as the droplet sizes progressively decreased, the importance of break-up mechanism on the DSD was reduced. When the equilibrium was reached, the main features of the distribution (see Table 5) were almost identical whatever the stirrer used. By comparing runs carried out with the same surfactant-to-oil ratio and with a lower, intermediate or high level of specific power input, there is no significant difference between average diameters. However considering the variation coefficient, the distribution tended to be narrower with the flat blade propeller since such axial flow impeller produced a flow pattern as a single loop throughout the entire tank, leading to better dissipation of the energy brought by the stirrer [41]. These observations with dilute emulsions are in accordance with the study of Zhou and Kresta [37] and Pacek et al. [39]. If it is aimed at producing a droplet size distribution as narrow as possible, the use of a Rushton turbine instead of a flat blade propeller does not bring about a decisive advantage. As the stabilized O/W dispersion could be crystallized by cooling in a second stage [42], the flat blade propeller used for liquid–solid homogeneization [41] appears to be a multipurpose stirrer allowing the achievement of the emulsification and of the crystallization by cooling with the same equipment.

4.3. Further comparison with the literature

4.3.1. Largest and smallest stable droplet sizes

The largest droplet size detected at equilibrium in the DSD could be compared to the maximum droplet diameter d_{max}, which may be predicted from Eq. (7) using the Weber number. For the runs performed with the Rushton turbine, the largest visualized sizes were in size class ranging from 78 µm to 84 µm; it represented <1% of the total number of droplets. d_{max} decreased from 118 µm to 89 µm depending on the stirring conditions (see values in Table 4). The maximal size is overestimated by about 30 µm with respect to the prediction of Eq. (7) for a low stirring rate. For higher values of stirring rate the agreement between Eq. (7) and the experiment is correct and the correlation remains applicable.

The smallest droplet diameters detected were in the size class ranging from 12 µm to 20 µm and it represented <0.1% of the droplet population. In the same time, the scale of the smallest eddies l_{micro} were in the range of 16–24 µm (see Table 4). The fraction of droplets having a diameter lower than this microscale was very low. Zhou and Kresta [43] have demonstrated for several

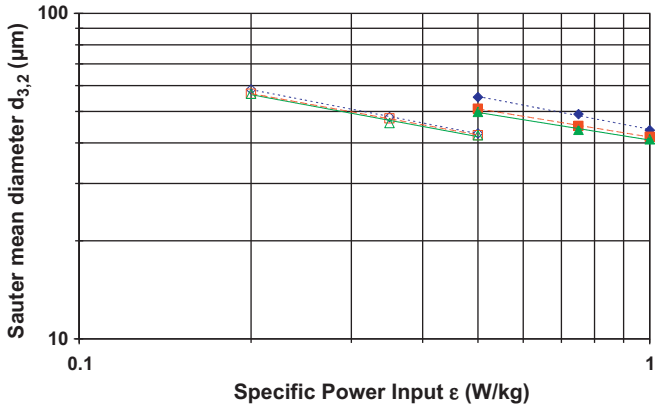

Fig. 8. Steady-state Sauter mean diameter $d_{3,2}$ for flat blade propeller (empty symbols) and Rushton turbine (full symbols) and for different surfactant-to-oil ratios (♦: 0.1; ■: 0.5; ▲: 1.0).

impellers that the number of droplets smaller than the Kolmogorov length scale could be high when the specific power input was low, meaning that the coalescence does not operate and the break-up mechanism dominates in all the droplet size range. In this study, the absence of droplet smaller than the Kolmogorov microscale tends to demonstrate that the coalescence rate is significant for the smallest droplets and the turbulence dissipation rate brought by the stirring may ensure equilibrium between break-up and coalescence. Using this microscale l_{micro} as an estimate of the minimum drop size appears to be appropriate in this study.

4.3.2. Correlation between $d_{3,2}$ and ε

Eq. (8) correlates the Sauter mean diameter $d_{3,2}$ with the mean specific energy dissipation rate ε. For each surfactant-to-oil ratio and the two stirrers used, $d_{3,2}$ is plotted against ε in Fig. 8. The values of the exponents used in Eq. (8) given in Table 6 should be treated with caution since each value came from the regression of only 3 experimental data points. These experimental values were lower than the theoretical of −0.4, and differed from the ones presented by Pacek et al. [39] lying in the range −0.41 to −0.72 for six different stirrers. Such discrepancies between values seem to demonstrate that the assumptions used are not consistent with the present results. On the basis of an experimental study with several other stirrers Zhou and Kresta [43] have already questioned this correlation and the proportionality between $d_{3,2}$ and d_{max}.

Table 6
Values of exponent (Eq. (8)) for different stirrers and surfactant-to-oil ratios.

	Exponent of the expression (9)		
	TA/EGDS = 0.1	TA/EGDS = 0.5	TA/EGDS = 1.0
Flat blade propeller	−0.34	−0.32	−0.32
Rushton turbine	−0.34	−0.29	−0.28

4.3.3. Time to equilibrium and shape of the stable DSD

In their review, Leng and Calabrese [36] have reported several studies in the 90s in which the circulating time in a stirred vessel required for a dilute dispersion to reach the equilibrium DSD was investigated. Emulsion droplets must pass through the high turbulence stirrer zone several times in order to be broken up progressively. The number of passes in the close vicinity of the stirrer in order to reach a stable DSD was estimated as about one thousand passes [36]. According to the stirring conditions of this study, the mean circulation time was in the range of 2.5–3.6 s (see Table 4). The times required to reach equilibrium DSD could then be assessed to 2500–3600 s which are about only one third to one quarter of the experimental ones (about 3 h). This large discrepancy may be explained by the evolution of the droplet size measurement technique. In the first hour of emulsification, the DSD changes very fast and its variation is easy to detect with the *ex situ* sizing techniques used in the early studies. After 1 h, the DSD evolution is much slower; the present investigation gives evidence of it using the *in situ* sizing probe. It is preferable to consider several (3–4) thousands of passes through the stirring zone in order to achieve the stabilization of the droplet size distribution.

Table 5
Number and volume droplet distribution features calculated from measurement.

Run number	Stirrer	Specific power input ε (W/kg)	Surfactant-to-oil ratio (weight)	Number size distribution		Volume size distribution		Mean Sauter diameter $d_{3,2}$ (µm)	$X_{mean} = d_{4,3}/d_{3,2}$ (–)
				Average size $d_{1,0}$ (µm)	Variation coefficient VC_N (–)	Average size $d_{4,3}$ (µm)	Variation coefficient VC_V (–)		
AK26	Flat blade Propeller	0.2	0.1	53.9	0.21	60.2	0.17	58.4	1.03
AK27		0.35		45.2	0.17	49.3	0.16	48.0	1.03
AK28		0.5		40.2	0.18	44.2	0.19	42.8	1.03
AK19		0.2	0.5	52.6	0.2	58.4	0.17	56.6	1.03
AK24		0.35		45.1	0.17	48.8	0.16	47.6	1.03
AK20		0.5		40	0.17	43.5	0.17	42.3	1.03
AK17		0.2	1.0	52.1	0.22	58.5	0.17	56.6	1.03
AK23		0.35		43.6	0.17	47.3	0.17	46.1	1.03
AK18		0.5		39.6	0.18	43.8	0.2	42.3	1.04

Run number	Stirrer	Specific power input ε (W/kg)	Weight ratio surfactant to EGDS	Number size distribution		Volume size distribution		Mean Sauter diameter $d_{3,2}$ (µm)	$X = d_{4,3}/d_{3,2}$ (–)
				Average size $d_{1,0}$ (µm)	Variation coefficient (–)	Average size $d_{4,3}$ (µm)	Variation coefficient (–)		
AK30	Rushton turbine	0.5	0.1	50	0.24	57.5	0.18	55.3	1.03
AK32		0.75		45	0.21	50.9	0.19	49.0	1.03
AK31		1		40	0.21	45.8	0.22	43.7	1.03
AK35		0.50	0.5	46.8	0.21	52.8	0.18	51.0	1.03
AK36		0.75		41.8	0.2	46.8	0.19	45.1	1.03
AK37		1.00		38.8	0.19	43.4	0.21	41.8	1.03
AK38		0.50	1	45.5	0.22	51.7	0.19	49.8	1.03
AK39		0.75		40.9	0.19	45.4	0.18	43.9	1.03
AK18		1.00		38	0.2	42.7	0.22	41.0	1.04

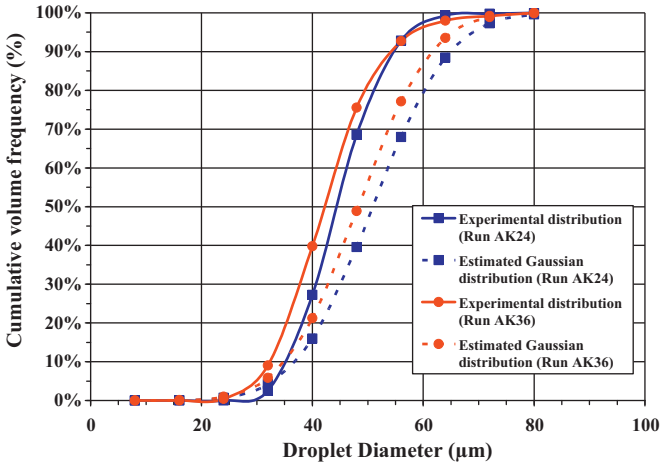

Fig. 9. Droplet size distribution at equilibrium for runs AK24 (■) and AK36 (●): comparison of the experimental distributions (solid line) and estimated Gaussian distributions (dotted line).

Authors have also worked on the prediction of the stable DSD once the $d_{3,2}$ has been estimated. It was assumed that the functional form of the DSD and its mean and standard deviation were weakly sensitive to the scale and geometry features of the stirred vessel [36]. For low viscosity dispersed phases, it was assumed that the volume distribution of droplet size exhibited a Gaussian shape, with values of the mean normalized size X_{mean} (expressed as the $d_{4,3}$ to $d_{3,2}$ ratio) and of the variation coefficient VC_V respectively equal to 1.07 and 0.24. The X_{mean} and the VC_V were calculated for each experimental stable DSD and are presented in Table 5. Fig. 9 displays the experimental volume DSD expressed as their cumulative form for two representative runs obtained with the two stirrers, and compares it to its estimated volume DSD. Whatever the operating conditions, the experimental values of X_{mean} (about 1.03) are close to the literature value. However, experimental values of VC_V were significantly lower than the proposed literature value. The extent of the experimental volume distribution appears narrower than predicted, which is clearly visualized in Fig. 9.

5. Conclusions and perspectives

An emulsification process of a dilute O/W emulsion carried out in a stirred vessel was monitored in real time with an *in situ* optical probe. The video sequences regularly recorded were automatically treated with an image analysis procedure based on a circular Hough transform allowing the estimation of diameters of several thousands of droplets. It is then possible to follow the evolution with time of the DSD. This experimental size monitoring was applied to an emulsion for which warm conditions must be maintained in order to prevent the solidification of the dispersed phase. This advantage has to be emphasized when the droplet size distribution of a crystallizable emulsion has to be measured. Moreover, thanks to the development of this *in situ* measurement technique coupled with an automatic image analysis treatment, the optimization of an emulsification process (in dilute conditions) in a laboratory reactor scaled down from an industrial stirred reactor was possible.

An increase of the specific power input brought by the stirrer allowed reducing the droplet diameter and the extent of the size distribution. It is the first order parameter influencing the final DSD since it plays a major role on the droplet break-up mechanism. To a lesser extent the increase of the surfactant amount had also a favorable impact on the reduction of the droplet diameter and on the narrowing the size distribution by its action on the coalescence rate and on the stabilization of O/W interface. It was a parameter of secondary relevance in this study. Final droplet distributions were similar whatever the stirrer employed. The Rushton turbine allowed a faster size reduction of the droplet diameter in the first hour of emulsification. On the contrary, the size distribution tended to be narrower with the flat blade propeller when the equilibrium regime was achieved. The use of a Rushton turbine instead of a flat blade propeller does not bring about a decisive advantage for the production of a droplet distribution of several tens of microns. Moreover, the flat blade propeller appears a better multipurpose stirrer since it could be used for the crystallization of the dispersed oil phase at lower temperatures.

The agreement between the largest droplet size and the maximum droplet diameter estimated with a correlation based on the Weber number is obtained for high stirring rate. The agreement was also obtained between the smallest droplet diameter measured and the smallest size of eddies estimated with the Kolmogorov microscale. The prediction proposed in the literature could be applied in this study. On the other hand, the time to obtain a stable DSD tends to be underestimated in the literature by a factor of 3–4. The knowledge of this time required to reach to equilibrium regime is important when the control of a process needs a reproducible size distribution from batch to batch.

From this study, future studies will be done in two directions. Firstly the examination of the experimental data does not allow one to fully explain the course of the emulsification process. One could hardly go further in the assumptions concerning the break-up and coalescence mechanisms involved because these latter cannot be completely differentiated. The kinetic features of the emulsification process governing the final droplet size distribution may be assessed through a detailed modelling of the experimental results designed using a population balance equation coupled with break-up and coalescence equations. Secondly this new *in situ* optical probe will be used at lower temperature than 70 °C in order to determine the solidification frequency of the dispersed melted phase according to the droplet diameter. This point has to be investigated when the control of a crystallizable emulsion process is required.

Acknowledgments

The support of the Ministère de l'Enseignement Supérieur et de la Recherche is gratefully acknowledged. In addition the authors are indebted to P. Buffin and R. Henry for their help in the experimental part of this study.

References

[1] P. Becher, Emulsions: Theory and Practice, 3rd ed., Oxford University Press, New York, 2001.
[2] D. Moinard-Checot, Y. Chevalier, S. Briançon, H. Fessi, S. Guinebretière, Nanoparticles for drug delivery: review of the formulation and process difficulties illustrated by the emulsion–diffusion process, J. Nanosci. Nanotechnol. 6 (9–10) (2006) 2664–2681.
[3] J. Frelichowska, M.-A. Bolzinger, J. Pelletier, J.-P. Valour, Y. Chevalier, Topical delivery of lipophilic drugs from o/w pickering emulsions, Int. J. Pharm. 371 (2009) 56–63.
[4] R.L. Crombie, Cold pearl surfactant-based blends, Int. J. Cosmet. Sci. 19 (1997) 205–214.
[5] A.M. O'Rourke, P.F. MacLoughlin, A study of drop breakage in lean dispersions using the inverse-problem method, Chem. Eng. Sci. 65 (11) (2010) 3681–3694.
[6] S. Maaβ, S. Wollny, A. Voigt, M. Kraume, Experimental comparisons of measurement techniques for drop size distributions in liquid/liquid dispersions, Exp. Fluids, in press.
[7] D. Ramkrishna, Population Balances – Theory and Applications to Particulate Systems in Engineering, Academic Press, San Diego, 2000, doi:10.1007/s00348-010-9.
[8] J. Floury, J. Bellettre, J. Legrand, A. Desrumaux, Analysis of a new type of high pressure homogeniser: a study of the flow pattern, Chem. Eng. Sci. 59 (4) (2004) 843–853.

[9] J. Floury, J. Legrand, A. Desrumaux, Analysis of a new type of high pressure homogeniser: part B: study of droplet break-up and recoalescence phenomena, Chem. Eng. Sci. 59 (6) (2004) 1285–1294.
[10] N. Vankova, S. Tcholakova, N. Denkov, I. Ivanov, V. Vulchev, T. Danner, Emulsification in turbulent flow—1. Mean and maximum drop diameters in inertial and viscous regimes, J. Colloid Interface Sci. 312 (2) (2007) 363–380.
[11] N. Vankova, S. Tcholakova, N. Denkov, V. Vulchev, Emulsification in turbulent flow 2. Breakage rate constants, J. Colloid Interface Sci. 313 (2) (2007) 612–629.
[12] S. Tcholakova, N. Vankova, N. Denkov, T. Danner, Emulsification in turbulent flow: 3. Daughter drop-size distribution, J. Colloid Interface Sci. 310 (2) (2007) 570–589.
[13] N.B. Raikar, S.R. Bhatia, M.F. Malone, M.A. Henson, Experimental studies and population balance equation models for breakage prediction of emulsion drop size distributions, Chem. Eng. Sci. 64 (2009) 2433–2447.
[14] A.N. Sathyagal, D. Ramkrishna, G. Narsimhan, Droplet breakage in stirred dispersions: breakage functions from experimental drop size distributions, Chem. Eng. Sci. 51 (1996) 1377–1391.
[15] A.M. O'Rourke, P.F. MacLoughlin, A comparison of measurement techniques used in the analysis of evolving liquid–liquid dispersions, Chem. Eng. Process. 44 (2005) 885–894.
[16] D.A.R. Brown, P.N. Jones, J.C. Middleton, Part A: measuring tools and techniques for mixing and flow visualization studies, in: E.L. Paul, V.A. Atiemo-Obeng, S.M. Kresta (Eds.), Handbook of Industrial Mixing, Handbook of Industrial Mixing, John Wiley & Sons, New Jersey, 2004, pp. 145–201.
[17] E. Hukkanen, R. Braatz, Measurement of particle size distribution in suspension polymerization using in situ laser backscattering, Sens. Actuators B: Chem. 96 (1–2) (2003) 451–459.
[18] D. Greaves, J. Boxall, J. Mulligan, A. Montesi, J. Creek, E.D. Sloan, C.A. Koh, Measuring the particle size of a known distribution using the focused beam reflectance measurement technique, Chem. Eng. Sci. 63 (2008) 5410–5419.
[19] A.W. Pacek, I.P.T. Moore, A.W. Nienow, R.V. Calabrese, Video technique for measuring dynamics of liquid–liquid dispersion during phase inversion, AIChE J. 40 (12) (1994) 1940–1949.
[20] A.W. Pacek, A.W. Nienow, I.P.T. Moore, On the structure of turbulent liquid–liquid dispersed flows in a agitated vessel, Chem. Eng. Sci. 49 (20) (1994) 3485–3498.
[21] J. Ritter, M. Kraume, On line measurement technique for drop size distribution in liquid/liquid systems at high dispersed phase fractions, Chem. Eng. Technol. 23 (2000) 579–581.
[22] F.B. Alban, S. Sajjadi, M. Iianneskis, Dynamic tracking of fast liquid-liquid dispersion processes with real time in situ optical technique, Chem. Eng. Res. Des. 82 (A8) (2004) 1054–1060.
[23] E. Gagniere, D. Mangin, F. Puel, O. Monnier, E. Garcia, J.-P. Klein, Formation of Co-crystals: kinetic and thermodynamic aspects, J. Cryst. Growth 311 (2009) 2689–2695.
[24] C. Subero-Couroyer, D. Mangin, A. Rivoire, A.F. Blandin, J.-P. Klein, Agglomeration in suspension of salicylic acid fine particles: analysis of the wetting period and effect of the binder injection mode on the final agglomerate size, Powder Technol. 161 (2) (2006) 98–109.
[25] T. Peng, A. Balijepalli, S.K. Gupta, T. LeBrun, Algorithms for on-line monitoring of micro spheres in an optical tweezers-based assembly cell, transactions of the ASME, J. Comp. Inform. Sci. I7 (2007) 330–338.
[26] J. Illingworth, J. Kittler, The adaptive Hough transform, IEEE Trans. Pattern Anal. Mach. Intell. 9 (5) (1987) 690–698.
[27] J. Illingworth, J. Kittler, A survey of the Hough transform, Comput. Vision, Graphics Image Process. 44 (1988) 87–116.
[28] W. Bujalski, A.W. Nienow, S. Chatwin, M. Cooke, The dependency on scale of power numbers of Rushton disc turbines, Chem. Eng. Sci. 42 (1987) 317–326.
[29] M. Roustan, Agitation, Mélange Caractéristiques des mobiles d'agitation Techniques de l'Ingénieur J3802 (2005) 1–12.
[30] M. Roustan, J.-C. Pharamond, A. Line, Agitation, Mélange Concepts théorique de base Techniques de l'ingénieur J3800 (1999) 1–22.
[31] A.N. Kolmogorov, The local structure of turbulence in incompressible viscous fluid for very large Reynolds numbers, Doklady Akademii Nauk SSSR 30 (1941) 301–305.
[32] C.A. Coulaloglou, L.L. Tavlarides, Drop size distributions and coalescence frequencies of liquid–liquid dispersions in flow vessels, AIChE J. 22 (2) (1976) 289–297.
[33] J.O. Hinze, Fundamentals of the hydrodynamic mechanism of splitting in dispersion processes, AIChE J. 1 (3) (1955) 289–295.
[34] R. Shinnar, On the behaviour of liquid dispersions in mixing vessels, J. Fluid Mech. 10 (2) (1961) 259–275.
[35] J.S. Lasigetty, P.K. Das, R. Kumar, Breakage of viscous and non-newtonian drops in stirred vessel, Chem. Eng. Sci. 41 (1) (1986) 65–72.
[36] D.E. Leng, R.V. Calabrese, Immiscible liquid–liquid systems, in: E.L. Paul, V.A. Atiemo-Obeng, S.M. Kresta (Eds.), Handbook of Industrial Mixing, Handbook of Industrial Mixing, John Wiley & Sons, 2004, pp. 639–754.
[37] G. Zhou, S.M. Kresta, Evolution of drop size distributions in liquid–liquid dispersions for various impellers, Chem. Eng. Sci. 53 (1998) 2099–2113.
[38] E. Chatzi, C.J. Boutris, C. Kiparissides, On line monitoring of drop size distributions. 1. Effects of temperature and impeller speed, Ind. Eng. Chem. Res. 30 (1991) 536–543.
[39] A.W. Pacek, S. Chamsart, A.W. Nienow, A. Bakker, The influence of impeller type on mean drop size and drop size distribution in an agitated vessel, Chem. Eng. Sci. 54 (1999) 4211–4222.
[40] E. Chatzi, C.J. Boutris, C. Kiparissides, On line monitoring of drop size distributions. 2. Effects of stabilizers concentration, Ind. Eng. Chem. Res. 30 (1991) 1307–1313.
[41] R.R. Hemrajani, G.B. Tatterson, Mechanically stirred vessels, in: E.L. Paul, V.A. Atiemo-Obeng, S.M. Kresta (Eds.), Handbook of Industrial Mixing, Handbook of Industrial Mixing, John Wiley & Sons, 2004, pp. 345–390.
[42] M.A. Bolzinger, L. Lafferrere, C. Cogne, F. Salvatori, P. Ardaud, M. Zanetti, F. Puel, Effects of surfactants on crystallization of ethylene glycol distearate in oil-in-water emulsion, Colloids Surfaces A: Physicochem. Eng. Aspects 299 (1–3) (2007) 93–100.
[43] G. Zhou, S.M. Kresta, Correlation of mean drop size and minimum drop size with the turbulence energy dissipation and the flow in an agitated tank, Chem. Eng. Sci. 53 (1998) 2063–2079.